Turkish Journal of Electrical Engineering & Computer Sciences

http://journals.tubitak.gov.tr/elektrik/

Research Article

Turk J Elec Eng & Comp Sci
(2017) 25: 1010 – 1020
© TÜBİTAK
doi:10.3906/elk-1507-1

Modeling lattice-matched InP-based multijunction solar cells

Tuğba Selcen NAVRUZ*
Department of Electrical & Electronics Engineering, Faculty of Engineering, Gazi University, Ankara, Turkey

Received: 01.07.2015 • **Accepted/Published Online:** 15.03.2016 • **Final Version:** 10.04.2017

Abstract: Currently, the multijunction solar cell structure gives the highest efficiency for photovoltaic solar cells. In this study, tandem, triple, and quadruple junction multijunction solar cell structures that include an InP subcell on InP substrate were investigated. A model that can calculate both the voltage–current characteristics and external quantum efficiency was demonstrated. The model gave fitted results with the experimental data for a single junction GaAs solar cell and a tandem solar cell that provides efficiency higher than 30%. The model was used to optimize the lattice-matched AlAsSb/InP tandem, AlAsSb/InP/InGaAsP triple, and AlAsSb/InP/InGaAsP/GaAsSb quadruple junction solar cell designs and the highest efficiencies obtained for these cells were 29.9%, 36.69%, and 42.79%, respectively, under AM1.5 spectrum without any sun concentration. This lattice-matched quadruple junction structure gives the opportunity of having high efficiency without wafer bonding.

Key words: Multijunction solar cell, modeling solar cell, high efficient solar cells

1. Introduction

The detailed balance efficiency limit for a p-n junction solar cell is about 30% under 1 sun illumination and 40% under maximum concentration [1]. The main factor that limits the efficiency is absorption of the solar spectrum inefficiently since the photons with energy lower than the bandgap of cell material cannot be absorbed and the excess energy of high energy photons is wasted thermally. A multijunction solar cell consisting of two or more stacked p-n junctions with different bandgaps can use a wider portion of the solar spectrum and therefore provides higher efficiency. The 1 sun detailed balance efficiency limit for a tandem solar cell is calculated as 45.71% under AM1.5 illumination where the optimum bandgaps of p-n junctions are E_{G1} = 0.94 eV and E_{G2} = 1.6 eV [2,3]. The theoretical efficiency limit for an infinite number of junctions is given as 86.8% [4].

III–V-based materials are mostly used for the realization of high efficient multijunction solar cells [5–9] whose world efficiency record is reported as 46% [10,11]. Ge-based multijunction solar cells are very common in the literature [7,9]. Lattice-matched and lattice-mismatched GaInP/InGaAs/Ge triple junction solar cells are classic examples for Ge-based solar cells with efficiency higher than 40% under concentration [9]. InP-based solar cells [11–13] have less application for multijunction solar cells since InP substrate is more expensive than Ge. However, the lattice constant of InP is more appropriate when the number of junctions is increased. The quadruple junction solar cell that provides the world record efficiency uses InP substrate [11]. Dimroth et al. connected two tandem cells by wafer bonding; where an InGaP/GaAs tandem cell on GaAs substrate was at the top and an InGaAsP/InGaAs tandem cell on InP substrate was at the bottom. The GaAs substrate was

*Correspondence: selcen@gazi.edu.tr

lifted off after the growing process. In the present study, all subcells were chosen so as to be lattice matched to InP. Thereby high efficiency was obtained on a single substrate and no wafer bonding was needed.

Deposition of one material on top of another is based on specific interface structures between the crystal lattices of the sequent layers (a_i and a_{i+1}). These interfaces are characterized by the lattice mismatch, f defined by, $f = (a_i - -a_{i+1})/a_i$ [14]. Since lattice mismatch prevents growth of defect-free structures, lattice-matched materials are mostly preferred for multijunction solar cells.

In order to design InP-based optimum tandem, triple, and quadruple junction solar cell structures, continuity equations and drift-diffusion current equations are used to model single junction solar cell at first. Current–voltage ($J - V_{OUT}$) characteristics and external quantum efficiency (EQE) curves under an AM1.5 spectrum for one sun concentration are calculated. Obtained results were in agreement with experimental data for single junction GaAs solar cells [15]. Then the model is improved for calculating the output characteristics of multijunction solar cell. The model is tested on InGaP/GaAs tandem cell [8] and it is seen that the results fitted the experimental data. Lastly, InP-based tandem, triple, and quadruple solar cell structures are modeled by optimizing the p and n side doping concentrations and thicknesses to achieve current matching and maximum efficiency.

Bremner et al. [2] reported the optimum bandgap values for a triple junction solar cell as 1.90, 1.37, and 0.94 eV, respectively. In this study, $AlAs_{0.56}Sb_{0.44}$ (E_G = 1.91 eV), InP (E_G = 1.34 eV), and InGaAsP (E_G = 1.1 eV) subcells whose bandgaps are close to optimum values are used for triple junction solar cell design. Finally, a $GaAs_{0.51}Sb_{0.49}$ (E_G = 0.787 eV) subcell is inserted as a fourth junction. The quadruple structure bandgap values are not the optimum values given in [2] but they are close to the ones that were used in [11].

2. Modeling multijunction solar cell

Drift-diffusion current equations combined with continuity equations that give the opportunity of including the effects of material parameters are the most common approach to model p-n junction and multijunction solar cells [16–18]. While modeling a p-n junction solar cell, electric field is assumed to be zero outside the depletion region. Therefore, diffusion current is dominant in the p and n regions, while drift current is dominant in the depletion region. The following equations are derived from continuity equations including radiative and nonradiative recombination terms and semiconductor diffusion current equations [19] for the p and n sides of the cell.

$$D_e \frac{d^2 \Delta n}{dx^2} - rg \frac{\Delta n}{n_{eq}} - \frac{\Delta n}{\tau_c} = -g_{eh} \tag{1}$$

$$D_h \frac{d^2 \Delta p}{dx^2} - rg \frac{\Delta p}{p_{eq}} - \frac{\Delta p}{\tau_v} = -g_{eh} \tag{2}$$

Here D_e and D_h are electron and hole diffusion coefficients. The Einstein relation exists between mobility and diffusion coefficient ($D/\mu = k_B T/q$, where k_B is the Boltzmann constant, T is cell temperature, which is assumed to be 300 K in this study, and q is electron charge). n_{eq} and p_{eq} are electron and hole minority concentrations under thermal equilibrium where Δn and Δp are excess electron and hole densities. The second and the third terms in the above equations represent radiative and Shockley–Read–Hall (SRH) recombination rates, respectively. τ_c and τ_v are SRH recombination lifetimes of electrons and holes and rg is the radiative

recombination coefficient given as below:

$$rg = \frac{2\pi}{h^3c^2}\int_0^\infty \alpha_{CV}(\varepsilon)\,\varepsilon^2 \exp(-\frac{\varepsilon}{k_B T_C})d\varepsilon \tag{3}$$

Here h represents the Planck constant, c is light velocity, ε is energy, and α_{CV} is the material absorption coefficient that changes with energy.

g_{eh} terms in Eqs. (1) and (2) are the photogeneration rate due to the transition of electrons from VB to CB by absorption of photons [19].

$$g_{eh}(x) = \int (1 - R(\varepsilon))\alpha_{CV}(\varepsilon)Nph(\varepsilon)\exp\left(-\alpha_{CV}(\varepsilon)x\right)d\varepsilon, \tag{4}$$

where R is reflectivity of the cell material due to the refractive index difference. Nph represents the number of photons per unit area per unit time for AM1.5 illumination and x is the distance that light travels through the material.

Eqs. (1) and (2) are solved using boundary conditions given below with the finite element method for short circuit (output voltage, $V_o = 0$) and dark ($g_{eh} = 0$) conditions:

$$\Delta n = n_{eq}\left(e^{\frac{qVo}{k_B T}} - 1\right) \quad \text{at} \quad x = w_p \tag{5a}$$

$$\Delta p = p_{eq}\left(e^{\frac{qVo}{k_B T}} - 1\right) \quad \text{at} \quad x = -wn \tag{5b}$$

$$D_n\frac{dn}{dx} = S_n\Delta n \quad \text{at} \quad x = xp \tag{5c}$$

$$-D_p\frac{dp}{dx} = S_p\Delta p \quad \text{at} \quad x = -xn \tag{5d}$$

For the above equations the junction is assumed to be at $x = 0$ point. x_p and x_n are the thicknesses of the p and n sides, respectively. w_p and w_n are the depletion region thicknesses formed on the p side and n side. S_n and S_p are surface recombination rate terms of electrons and holes, respectively.

Under short circuit condition, the photocurrent contribution of the n and p sides of the cell is obtained using the calculated Δn and Δp variations ($J_n = D_n d\Delta n/dx$, $J_p = -D_p d\Delta p/dx$). Under dark conditions, dark current variation with the output voltage (boundary conditions in Eqs. (5a) and (5b)) is calculated. The photo and dark current contribution of the depletion region is given as below:

$$J_{photo_dep} = -q\int_{-w_n}^{w_p}(g_{eh})dx \tag{6a}$$

$$J_{dark_dep} = -q\int_{-w_n}^{w_p}(-u_{rad} - u_{nr})dx \tag{6b}$$

Here u_{rad} and u_{nr} are radiative and nonradiative recombination rates depending on output voltage. Summing the short circuit condition contributions of the n side, p side, and depletion region, total photocurrent of the

cell is obtained. Similarly, total dark current is found by summing the dark current contributions of these three regions for varying values of output voltage. Finally, cell current–voltage variation hence the $J-V_{OUT}$ curve is obtained by subtracting the dark current from photocurrent and including the series (R_S) and shunt resistance (R_{SH}) effects [19].

$$J = J_{photo} - J_o e^{\frac{qV_o}{nk_BT}} - \frac{V_o}{AR_{SH}} \tag{7}$$

The second term on the right side of the above equation is the dark current contribution of the p-n junction, where J_o is the reverse saturation current and n is the ideality factor. Since the dark current variation with V_o is obtained from dark condition calculations, J_o and n can easily be extracted from that variation [20,21]. Here A is the surface area of the cell, which is assumed to be 1 cm^2, and V_o is the output voltage of the cell when series resistance effect is ignored. When it is taken into account, the final output voltage of the cell is given as follows:

$$V_{OUT} = V_o - JAR_S \tag{8}$$

Cell current density, J, for every value of $V_o$is obtained from Eq. (7) and V_{OUT} is found for every value of J from Eq. (8). Then the solar cell parameters;hort circuit current density (J_{sc}), open circuit voltage (V_{oc}), fill factor (FF), and efficiency (η) are determined.

The EQE curve is found from short circuit calculations.

$$EQE(\lambda) = \frac{J_{photo}(\lambda)}{qN_{ph}(\lambda)}, \tag{9}$$

where λ is wavelength and $\varepsilon= hc/\lambda$. $J_{photo}(\lambda)$ is calculated for every wavelength value by solving Eqs. (1)–(8) under short circuit condition without evaluating the integrals in Eqs. (3) and (4). EQE variation information enables us to know which part of the solar spectrum is being used efficiently. While designing multijunction solar cells, EQE variation is critical since the aim of this structure is to increase efficiency by absorbing a wider portion of the solar spectrum.

The model is applied to the GaAs single junction solar cell given in [15]. The calculated output parameters are nearly in agreement with the experimental data [15] as seen in Table 1. Optical parameters (n-k parameters) and electrical properties of GaAs are taken from [22]. SRH recombination life times of electrons and holes are assumed to be 25 ns and surface recombination rates Sn and Sp are assumed to be 2×10^3 and 10^2 cm/s, respectively [23].

Table 1. Experimental data and simulated results for GaAs single junction cell [15].

	Jsc (mA/cm^2)	Voc (V)	FF (%)	Efficiency (%)
Experimental data	20.5	1	83.5	17
Simulated data	20.3	1	83.5	16.95

After testing the single junction model, two, three, and four subcells are assumed to be serially connected via tunnel junctions. Similar to [23] we assumed the tunnel junction as an absorbing layer while calculating photocurrent and the electrical loss due to tunnel junction is taken into account as a series resistance element.

In order to evaluate the current–voltage characteristics of the multijunction solar cell, first photocurrent of serially connected subcells is calculated under short circuit condition. During the calculation, the effect of

absorption characteristics of the upper subcells to the lower ones is also included by changing the g_{eh} term. The generation rate of the nth subcell for n $>$ 1 is given as below assuming the top cell is the first subcell:

$$g_{eh_n}(x) = \exp(\sum_{i=1}^{n-1}(-\alpha_{CV_i}w_i - \alpha_{CV_ti}w_{ti})) \int (1-R_n)\alpha_{CV_n} Nph \exp(-\alpha_{CV_n}x)\, d\varepsilon \tag{10}$$

Here α_{CV_i} and α_{CV_ti} are the absorption coefficients of the ith subcell and tunnel diode, respectively, where w_i and w_{ti} correspond to the total thicknesses of the same layers. The short circuit current was chosen as the lowest photo-current of the subcells. Then the thicknesses are optimized to achieve current matching. Under dark conditions, the dark current component of the subcell cell with lowest bandgap is calculated first for varying values of subcell output voltage. Then the output voltages of other subcells are set to equalize the dark current component of all subcells. Total output voltage of the multijunction solar cell is the sum of subcell output voltages. Finally, both subcell and total current–voltage characteristics including series and shunt resistance losses are evaluated. Series resistance should be less than 0.1 Ω for high efficiency in solar cells. Therefore, we assumed series resistance to be 0.1 Ω and shunt resistance to be $1.5 \times 10^4 \Omega$ similar to [24]. *EQE* curves for each subcell are also obtained.

The multijunction model is tested on a tandem InGaP/GaAs solar cell [8] and, as seen from Table 2, the calculated data nearly fitted the experimental data. SRH coefficients and surface recombination terms are taken from [23].

Table 2. Experimental data and simulated results for InGaP/GaAs tandem cell [8].

	Jsc (mA/cm^2)	Voc (V)	FF (%)	Efficiency (%)
Experimental data	14.25	2.49	85.6	30.3
Simulated data	14.22	2.47	86.2	30.28

3. Results and discussion

The model described above is used to design lattice-matched AlAsSb/InP tandem, AlAsSb/InP/InGaAsP triple, and AlAsSb/InP/InGaAsP/GaAsSb quadruple multijunction solar cells on InP substrate. The material parameters for $AlAs_{0.56}Sb_{0.44}$, $In_{0.47}Ga_{0.53}As_{0.35}P_{0.65}$, and $GaAs_{0.51}Sb_{0.49}$ in the literature were very limited. Therefore, the available data for AlAs, AlSb [24–26], InP, InAs, GaP, GaAs, and GaSb [22] are used to calculate the required parameters by linear iteration [27]. In all designs, double layer antireflection coating [23] and $AlP_{0.39}Sb_{0.61}$ window layer are used. To best of the author's knowledge, the quadruple AlAsSb/InP/InGaAsP/GaAsSb structure is proposed and analyzed for the first time in this study. In addition, detailed structure design and *EQE* curve calculations are given for the first time in this study for AlAsSb/InP tandem and AlAsSb/InP/InGaAsP triple junctions. The proposed model is similar to previous ones but the radiative recombination rate variation due to wavelength is taken into account in this study, while most of the present models use radiative recombination term as a constant [28,29].

3.1. Tandem cell design

In the $AlAs_{0.56}Sb_{0.44}$/InP (1.91/1.34 eV) tandem structure, the AlAsSb top cell is optimized first and it is seen that photocurrent is maximized when total subcell thickness is 26 μm. In solar cell design, it is aimed to absorb all the photons with energy higher than the bandgap and to assure that the generated carriers can

contribute to the current. For nearly full absorption, absorption coefficient-cell thickness production $\alpha w \geq 5$ is required. On the other hand, thickness of the p and n sides cannot be larger than minority carrier diffusion length or the carriers will recombine before contributing to the cell current. Thus, an optimization is required about cell thickness. Since light absorption and hence electron-hole pair generation rate is faster in the upper layer, called the emitter, this layer is grown thinner with respect to the base layer. In this way most of the photogenerated carriers can reach the junction and contribute to cell current before recombining. In our design the optimum value of current contribution coming from the emitter is obtained as 9.75 mA/cm^2 for 1 μm thickness. It is seen that photocurrent is decreased if the emitter layer is thinner or thicker. If it is thinner there is not enough absorption and if it is thicker some of the carriers are lost. In the base layer, photon absorption and hence electron-hole generation is not so fast since the light is attenuated as it travels through the layers of the cell. Therefore, base layer thickness is grown larger to absorb the rest of the photons but again the recombination effect is taken into account and the optimum base thickness is obtained as 25 μm, which provides a 4.06 mA/cm^2 current. It is known that it is difficult to grow thick layers of $AlAs_{0.56}Sb_{0.44}$ in practice, but new growth technologies might be developed for this material in the future. Doping concentration is also an important parameter in solar cell design. A high doping concentration is necessary for high output voltage but increasing the doping concentration increases the recombination rate, and so decreases the life time and diffusion length of carriers. Therefore, in our all designs the thin emitter layer is highly doped and the thick base layer is lightly doped. The bottom InP subcell has the capability of providing higher photocurrent but its thickness is optimized to give the same current with the top subcell as seen in Table 3. The emitter layer is thin and highly doped and the base layer is thick and lightly doped as the top subcell. The output parameters and the current–voltage characteristics are presented in Table 4 and Figure 1a. As shown in Figure 1a, the output voltage of the tandem cell is the sum of the output voltages of the subcells. The performance of this tandem design is very close to that of the InGaP/GaAs tandem cell given in [8].

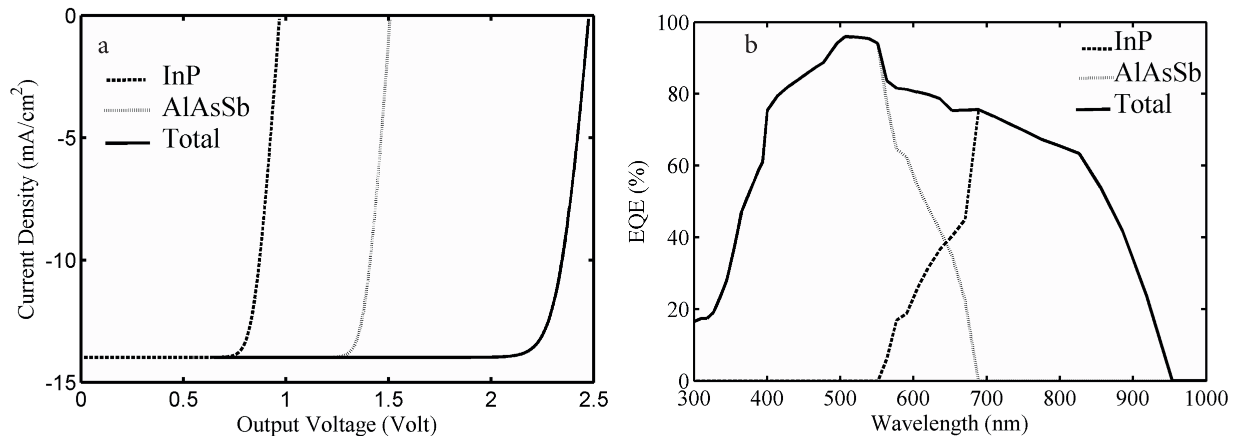

Figure 1. a) J-V curve of AlAsSb/InP tandem solar cell. b) *EQE* variation of AlAsSb/InP tandem solar cell.

The *EQE* curves of the proposed tandem cell are obtained as shown in Figure 1b. The AlAsSb top subcell begins to absorb photon at approximately 680 nm but *EQE* is quite low between 600 and 680 nm. This part of the spectrum was not absorbed since absorption coefficient values are quite low in this region and the thickness of the top subcell was limited due to the recombination effects. *EQE* is above 80% between 420 and 550 nm and decreases sharply for $\lambda <$ 420 nm due to the effect of the window layer. The absorption coefficient is higher and so absorption is very fast at low wavelengths (high energies). For this reason, the window layer absorbs

almost all of the high energy photons even though it is very thin. Although the window layer decreases the short circuit current of the cell, it is obligatory to minimize the effect of surface recombination. The InP subcell begins to absorb photons at nearly 950 nm. *EQE* is higher than 60% between 700 and 880 nm and decreases for higher energies since that portion of the spectrum is absorbed by the AlAsSb layer. The *EQE* values of the InP subcell are not as high as the top cell values since the thickness of the InP subcell is thinned to provide current matching. Therefore, that part of the solar spectrum cannot be fully absorbed. While modeling triple and quadruple junction solar cells, the unused part of the spectrum will be absorbed by the lower subcells.

Table 3. AlAsSb/InP tandem solar cell structure.

MgF_2/ZnS AR			
Layer	Material	Thickness (μm)	Doping (cm^{-3})
Window	$AlP_{0.39}Sb_{0.61}$	0.02	n-type C > 10^{19}
Emitter	$AlAs_{0.56}Sb_{0.44}$	1	n-type C = 10^{18}
Base	$AlAs_{0.56}Sb_{0.44}$	25	p-type C = 10^{17}
Tunnel	$AlAs_{0.56}Sb_{0.44}$	0.015	p-type Degenerate
Tunnel	$AlAs_{0.56}Sb_{0.44}$	0.015	n-type Degenerate
Emitter	InP	0.08	n-type C = 10^{18}
Base	InP	0.25	p-type C = 10^{17}

Table 4. AlAsSb/InP tandem solar cell output parameters.

Jsc (mA/cm^2)	Voc (V)	FF (%)	Efficiency (%)	$J_{OAlAsSb}/J_{OInP}$ (mA/cm^2)	n_{AlAsSb}/n_{InP}
13.98	2.48	86.2	29.9	$7.34 \times 10^{-26}/4.84 \times 10^{-18}$	1.08/1.05

3.2. Triple junction cell design

In the $AlAs_{0.56}Sb_{0.44}/InP/In_{0.47}Ga_{0.53}As_{0.35}P_{0.65}$ (1.91/1.34/1.1 eV) triple junction structure, an InGaAsP third subcell with 550 nm emitter and 1000 nm base thickness is added to the bottom of the previous structure where emitter and base doping concentrations are 10^{18} cm^{-3} and 10^{17} cm^{-3}, respectively. The emitter and base layers are optimized to provide current matching. Since the absorption coefficient increases with energy and the higher energy photons are absorbed by upper cells, photogeneration rate is a little bit slow with respect to the upper subcells. Therefore, the cell thickness for sufficient absorption is larger. Current voltage characteristics, *EQE* curves, and output parameters of the proposed solar cell are given in Figures 2a and 2b and Table 5, respectively. This design achieves an efficiency of 36.69%, which is higher than InGaP/InGaAs/Ge triple junction solar cell efficiency [9] under one sun illumination. The amounts of photocurrent provided by these two cells are very close to each other. However, the output voltage of the structure proposed here is higher since the bandgap and hence the contribution to the output voltage of the bottom InGaAsP cell is larger than that of the Ge subcell.

A large amount of overlap between InP and InGaAsP subcell *EQE* curves is seen in Figure 2b. InP subcell thickness was thinned for current matching in the tandem cell design. The unused part of the spectrum that InP subcell could not absorb is absorbed by the InGaAsP subcell in this triple cell design and the total *EQE* is increased. By this way the bottom subcell still achieves sufficient absorption and photocurrent, even though its bandgap is slightly higher than the optimum bandgap of 0.94 eV [2]. The spectrum between 300 and 1200 nm is absorbed in the proposed design. As the absorbed part of the spectrum increases, the efficiency also increases.

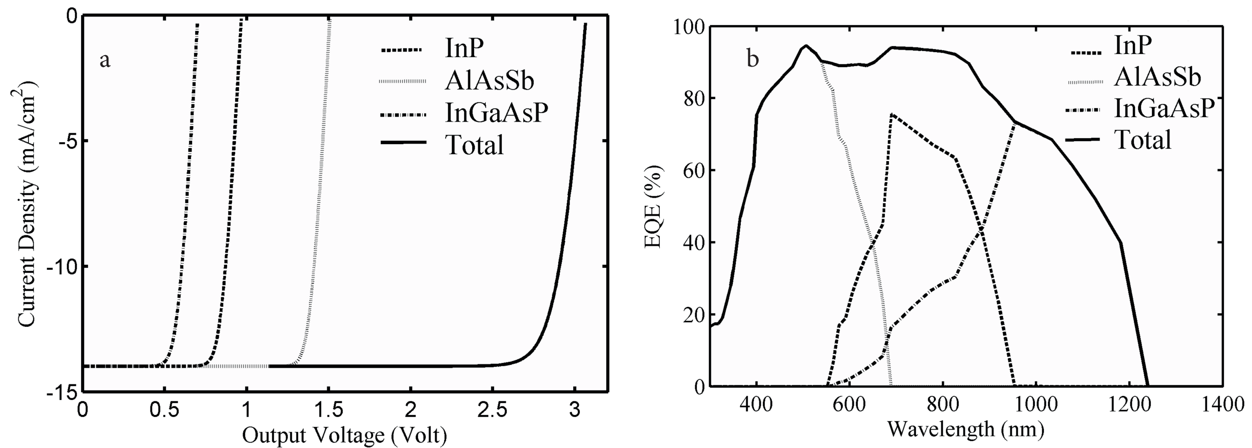

Figure 2. a) J-V curve of AlAsSb/InP/InGaAsP triple junction solar cell. b). *EQE* variation of AlAsSb/InP/InGaAsP triple junction solar cell.

Table 5. AlAsSb/InP/InGaAsP triple junction solar cell output parameters.

Jsc (mA/cm^2)	Voc (V)	FF (%)	Efficiency (%)
13.98	3.05	86.1	36.69

3.3. Quadruple junction cell design

In the $AlAs_{0.56}Sb_{0.44}$/InP/$In_{0.47}Ga_{0.53}As_{0.35}P_{0.65}$/$GaAs_{0.51}Sb_{0.49}$ (1.91/1.34/1.1/0.787 eV) quadruple junction structure, a GaAsSb fourth subcell with 600 nm emitter and 3500 nm base thickness is added to the bottom of the triple junction structure where emitter and base doping concentrations are 10^{18} cm^{-3} and 10^{17} cm^{-3}, respectively. The thicknesses are adjusted to provide current matching. A similar structure is given in [30] but the fourth cell is InGaAs in [30] and GaAsSb in this study. Moreover, in this study, optimum layer thicknesses, doping concentrations, and *EQE* variation, which are very important for multijunction solar cell design, are presented while no detailed analysis is presented in [30]. Another difference is AM0 (space applications) calculations are carried out in [30] where AM1.5 (terrestrial applications) calculations are presented here.

Current voltage characteristics, *EQE* curves, and output parameters of the proposed solar cell are given in Figures 3a and 3b and Table 6, respectively. The achieved efficiency by this quadruple junction solar cell is obtained as 42.79% without any sun concentration. If the variation of carrier life times, mobilities, and other parameters due to high sun concentration are ignored and if the photocurrent is assumed to increase linearly with concentration, the efficiency of our structure under 297 sun is 50.7%, which is higher than the world record efficiency [11].

Table 6. AlAsSb/InPInGaAsP/GaAsSb quadruple junction solar cell output parameters.

Jsc (mA/cm^2)	Voc (V)	FF (%)	Efficiency (%)
13.98	3.6	85.0	42.79

A very large part of the spectrum (300–1750 nm) is absorbed in this structure as seen from Figure 3b. There is a large amount of overlap between GaAsSb and InGaAsP subcells, which means that the fourth subcell absorbs the photons that are not absorbed by the upper cell.

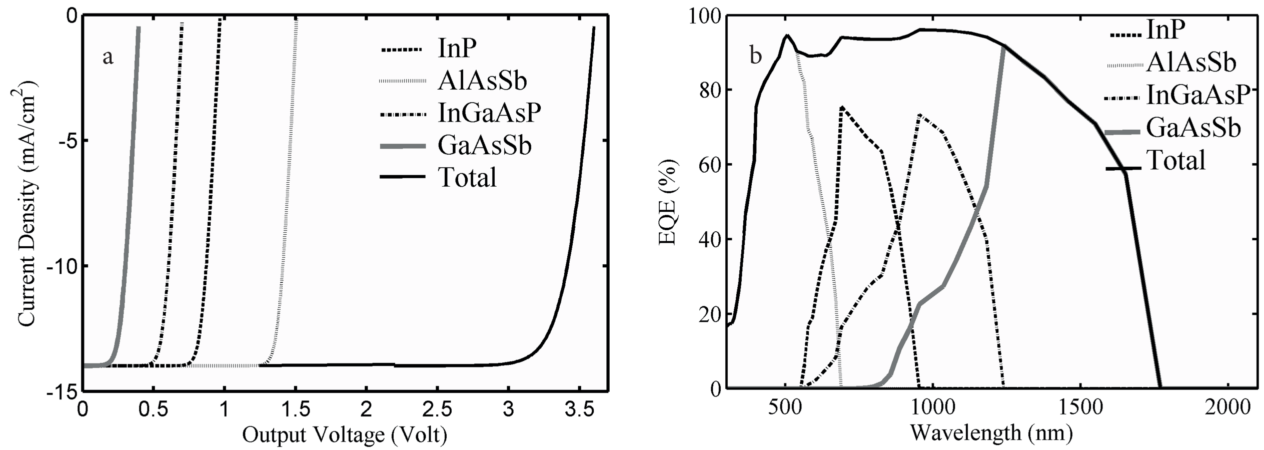

Figure 3. a) J-V curve of AlAsSb/InP/InGaAsP/GaAsSb quadruple junction solar cell. b) EQE variation of AlAsSb/InP/InGaAsP/GaAsSb quadruple junction solar cell.

The reverse saturation current density and ideality factor values extracted from dark current variation for all subcells are presented in Table 7.

Table 7. Reverse saturation current and ideality factor values of AlAsSb, InP, InGaAsP, and GaAsSb subcells.

	AlAsSb subcell	InP subcell	GaInAsP subcell	GaAsSb subcell
J_o (mA/cm^2)	7.6×10^{-22}	7.6×10^{-12}	1.6×10^{-9}	1.8×10^{-3}
n	1.13	1.29	1.17	1.57

4. Conclusions

In this study, InP-based AlAsSb/InP tandem, AlAsSb/InP/InGaAsP triple, and AlAsSb/InP/InGaAsP/GaAsSb quadruple junction solar cells are modeled under AM1.5 spectrum. Optimum doping concentrations and p- and n-side thicknesses providing current matching are found and current–voltage characteristics and EQE curves are obtained for each design. Since all the subcells are lattice matched no wafer bonding is needed. Furthermore, the proposed models give pretty high one sun efficiencies of 29.9%, 36.69%, and 42.79% for the tandem, triple, and quadruple junction designs, respectively. However, our model suffers from an insufficient database. If the optical and electrical properties of AlAsSb, InGaAsP, and GaAsSb calculated by iteration in this study are known exactly, more accurate results can be obtained. In any case, the presented results would be useful during the realization of InP-based multijunction solar cells.

References

[1] Shockley W, Queisser HJ. Detailed balance limit of efficiency of p-n junction solar cells. J Appl Phys 1961; 32: 510-519.

[2] Bremner SP, Levy MY, Honsberg CB. Analysis of tandem solar cell efficiencies under AM1.5g spectrum using a rapid flux calculation method. Prog Photovolt: Res Appl 2008; 16: 225-233.

[3] Alharbi FH, Kais S. Theoretical limits of photovoltaics efficiency and possible improvements by intuitive approaches learned from photosynthesis and quantum coherence. Renew Sust Energ Rev 2015; 43: 1073-1089.

[4] Tobías I, Luque A. Ideal efficiency of monolithic, series-connected multijunction solar cells. Prog Photovolt: Res Appl 2002; 10: 323-329.

[5] Lantratov VM, Kalyuzhnyoe NA, Mintairov NA, Timoshina NK, Shvarts MZ, Andreev VM. High-efficiency dual-junction GaInP/GaAs tandem solar cells obtained by the method of MOCVD. P Soc Photo-Opt Ins 2007; 41: 751-755.

[6] Bosi M, Pelosi C. The potential of III-V semiconductors as terrestrial photovoltaic devices. Prog Photovolt: Res Appl 2007; 15: 51-68.

[7] King RR, Bhusari D, Larrabee D, Liu XQ, Rehder E, Edmondson K, Cotal H, Jones RK, Ermer JH, Fetzer CM et al. Solar cell generations over 40% efficiency. Prog Photovolt: Res Appl 2012; 20: 801-815.

[8] Takamoto T, Ikeda E, Kurita H, Ohmori M. Over 30% efficient InGaP/GaAs tandem solar cells. Appl Phys Lett 1997; 70: 381-383.

[9] King RR, Law DC, Edmondson KM, Fetzer CM, Sherif RA, Kinsey GS, Krut DD, Cotal HL, Karam NH. Metamorphic and lattice-matched solar cells under concentration. In: IEEE 2006 4th World Conference on Photovoltaic Energy Conversion; 7–12 May 2006; Waikoloa, HI, USA: IEEE. pp. 760-763.

[10] Green MA, Emery K, Hishikawa Y, Warta W, Dunlop ED. Solar cell efficiency tables (Version 45). Prog Photovolt: Res Appl 2015; 23: 1-9.

[11] Dimroth F, Grave M, Beutel P, Fiedeler U, Karcher C, Tibbits TND, Oliva E, Siefer G, Schachtner M, Wekkeli A et al. Wafer bonded four-junction GaInP/GaAs//GaInAsP/GaInAs concentrator solar cells with 44.7% efficiency. Prog Photovolt: Res Appl 2014; 22: 277-282.

[12] Woo RL, Hong WD, Atwater HA, Law DC. High-efficiency InP-based multijunction solar cells. P Soc Photo-Opt Ins 2003; 5260: 110-113.

[13] Woo RL, Hong WD, Mesropian S, Leite MS, Atwater HA, Law DC. First demonstration of monolithic InP-based InAlAs/InGaAsP/InGaAs triple junction solar cells. In: IEEE 2011 Photovoltaic Specialists Conference; 19–24 June 2011; Seattle, WA, USA: IEEE. pp. 000295-000298.

[14] Trampert A, Brandt O, Ploog KH. Crystal structure of Group III Nitrides. San Diego, CA, USA: Academic Press, 1998.

[15] Philipps SP, Stetter D, Hoheisel R, Hermle M, Dimroth F, Bett AW. Characterization and numerical modeling of the temperature-dependent behavior of GaAs solar cells. In: 23rd European Photovoltaic Solar Energy Conference; 1–5 September 2008; Valencia, Spain: PVSEC. pp. 114-117.

[16] Baudrit M, Algora C. Modeling of GaInP/GaAs dual junction solar cells including tunnel junction. In: IEEE 2008 Photovoltaic Specialists Conference; 11–16 May 2008; San Diego, CA, USA: IEEE. pp. 1-5.

[17] Amine A, Mir Y, Zazoui M. Modelling of dual-junction solar cells including tunnel junction. Adv Cond Matter Phys 2013; 54632: 1-5.

[18] Lumb MP, González M, Bailey CG, Vurgaftman I, Meyer JR, Abell J, Yakes M, Hoheisel R, Tischler JG, Stavrinou PN et al. Drift-diffusion modeling of InP-based triple junction solar cells. P Soc Photo-Opt Ins 2013; 8620: 1-9.

[19] Nelson J. Physics of Solar Cells. London, UK: Imperial College Press, 2008.

[20] Singh NS, Jain A, Kapoor A. Determination of the solar cell junction ideality factor using special trans function theory (STFT). Sol Energ Mat Sol C 2009; 93: 1423-1426.

[21] Jain A, Kapoor A. A new method to determine the diode ideality factor of real solar cell using Lambert W-function. Sol Energ Mat Sol C 2005; 85: 391-396.

[22] Levinshtein M, Rumyantsev S, Shur M. Handbook Series on Semiconductor Parameters vol 1. London, UK: World Scientific, 1996.

[23] Connolly JP, Mencaraglia D, Renard C, Bouchier D. Designing III–V multijunction solar cells on silicon. Prog Photovolt: Res Appl 2014; 22: 810-820.

[24] Cotal H, Fetzer C, Boisvert J, Kinsey G, King R, Hebert P, Yoon H, Karam N. III–V multijunction solar cells for concentrating photovoltaics. Energy Environ Sci 2009; 2: 174-192.

[25] Kiehl RA, Gerhard STCL. High Speed Heterojunction Devices 41. San Diego, CA, USA: Academic Press, 1994.

[26] Tiwari S, Frank DJ. Empirical fit to band discontinuities and barrier heights in III–V alloy systems. App Physc Lett 1992; 60: 630-632.

[27] Gudeny M, Piprek J. Material parameters of quaternary III–V semiconductors for multilayer mirrors at 1.55 μm wavelength. Model Simul Mater Sc 1996; 4: 349-357.

[28] Gauffier A, David JP, Gilard O. Analytical model for multi-junction solar cells prediction in space environment. Microelectron Reliab 2008; 48: 1494-1499.

[29] Babar M, Rizvi AA, Al-Ammar EA, Malik NH. Analytical model of multi-junction solar cell. Arab J Sci Eng 2014; 39: 547-555.

[30] Gu Y. Design, fabrication and characterization of hetero-pn-junction devices for photovoltaic and photodedection applications. PhD, University of Maryland, Baltimore County, USA, 2008.